Journal of Computer Assisted Tomography
26(2):250–256

Diffusion-Weighted Echo Planar Imaging of Ovarian Tumors: Is It Useful to Measure Apparent Diffusion Coefficients?

Motoyuki Katayama, Takayuki Masui, Shigeru Kobayashi, Tatsuhiko Ito, Harumi Sakahara, Atsushi Nozaki, and Hiroyuki Kabasawa

Purpose: Our goal was to test the hypothesis, as previously reported in other studies, that apparent diffusion coefficients (ADCs) provide specific information to diagnose ovarian tumors, especially to discriminate between benign and malignant lesions.

Method: T1- and T2-weighted spin echo imaging and diffusion-weighted echo planar imaging were performed in 31 women with 61 cystic components of ovarian tumors.

Results: The lesions that showed typical watery intensity, hypointensity in T1-weighted imaging, and hyperintensity in T2-weighted imaging had similar ADCs, ranging from 1.54 to 1.84 × 10^{-3} mm^2 /s. The lesions that showed signal intensity different from typical watery intensity in conventional MRI tended to have low ADCs. In endometrial cysts, the mean ADC of the subgroup that showed typical watery intensity was higher than that of other subgroups.

Conclusion: With conventional MRI, a tendency of ADCs could be predicted. ADCs may not provide additional information, especially to discriminate benign from malignant lesions.

Index Terms: Ovary—Echo planar imaging.

INTRODUCTION

Magnetic resonance imaging has played an important role in diagnosis of ovarian tumors (1–4). Especially important clues are signal intensities in the fluid contents on T1- and T2-weighted MR images with and without fat suppression. One of the criteria to diagnose dermoid cysts is the detection of fat-suppressed contents with the fat-suppressed technique (5). Endometrial cysts are diagnosed on the specific findings of multiple cystic components, which showed hyperintensity on T1-weighted images and hypointensity on T2-weighted images (6,7). In routine clinical settings, however, it is sometimes difficult to make a diagnosis of cystic tumors with only T1- and T2-weighted images.

Water self-diffusion is the thermally induced behavior of water molecules moving in a microscopic random pattern, which is known as Brownian movement. Diffusion-weighted MRI is sensitive to this microscopic motion (8). Moteki and colleagues (9–11) evaluated the diagnostic performance of MRI for cystic ovarian tumors using apparent diffusion coefficients (ADCs). They reported that the cystic components of endometrial cysts and malignant ovarian tumors had lower ADCs than other lesions did. However, they provided no clear information about the relationship between signal intensities on T1- and T2-weighted imaging and ADCs for each cystic component. It is useful to clarify the relationship between signal intensities in T1- and T2-weighted imaging and ADCs for each cystic component. Then, we may be able to understand when we should use diffusion-weighted MRI for ovarian tumors in routine clinical examination and whether ADCs are useful to diagnose cystic ovarian tumors.

The purpose of this study was to clarify the relationship between the signal intensities in T1- and T2-weighted imaging and ADCs for the cystic components of the ovarian tumors and to evaluate the supplementary use of ADCs, especially to discriminate between benign and malignant lesions.

MATERIALS AND METHODS

Patients

During the 14-month period from July 1998 to August 1999, we performed diffusion-weighted echo planar im-

From the Department of Radiology, Seirei Hamamatsu General Hospital (M. Katayama, T. Masui, S. Kobayashi, and T. Ito), and Department of Radiology, Hamamatsu University School of Medicine (H. Sakahara), Shizuoka, and Application Research Group, GE Yokogawa Medical Systems, Tokyo (A. Nozaki and H. Kabasawa), Japan. Address correspondence and reprint requests to Dr. M. Katayama at Department of Radiology, Seirei Hamamatsu General Hospital, 2-12-12 Sumiyoshi, Hamamatsu, 430-8558, Japan. E-mail: mkataya@sis.seirei.or.jp

aging in 45 patients who were suspected of having ovarian tumors. Among them were 31 patients who underwent pelvic laparotomy or laparoscopy after MRI. The mean age was 39.1 years, ranging from 20 to 61 years. The final pathologic diagnoses were dermoid cysts (n = 10), endometrial cysts (n = 9), serous cystadenoma (n = 1), mucinous cystadenoma including borderline malignancy (n = 4), endometrial adenocarcinoma (n = 1), clear cell adenocarcinoma (n = 3), and serous adenocarcinoma (n = 3).

MR Protocol

MRI was performed on a 1.5 T magnet (Horizon LX Echo-Speed; GE Medical Systems, Milwaukee, WI, U.S.A.) with a torso phased array multicoil (GE).

The imaging protocol comprised (a) T2-weighted fast spin echo imaging in the sagittal plane with chemical shift-selective fat saturation pulse using the following imaging parameters: TR of 4,000 ms, effective TE of 85 ms, echo train length of 16, slice thickness of 5 mm with a 1 mm interslice gap, receiver bandwidth of 32 kHz, matrix of 256 × 256 with 512 zero fill interpolation (ZIP) (apparent in-plane resolution of 512 × 512), FOV of 26 × 19 cm, and NEX of 2. Imaging time was 2 min 8 s for 20 slices. (b) T1-weighted fast spin echo imaging in the axial plane without chemical shift-selective fat saturation pulse using the following imaging parameters: TR of 600 ms, TE of 11 ms, echo train length of 3, slice thickness of 7 mm with a 2 mm interslice gap, receiver bandwidth of 20.8 kHz, matrix of 256 × 192 with ZIP (apparent in-plane resolution of 512 × 512), rectangular FOV of 26 × 19 cm with 70% rectangular FOV technique, and NEX of 1. Imaging time was 1 min for 19 slices. (c) T1-weighted fast spin echo imaging in the axial plane with chemical shift-selective fat saturation pulse using the same parameters as T1-weighted imaging without chemical shift-selective fat saturation. Imaging time was 1 min 31 s for 19 slices. (d) Diffusion-weighted imaging with the single section spin echo type single shot echo planar sequence in the sagittal plane using the following parameters: TR of 4,999 ms, effective TE of 99 ms, thickness of 7 mm, bandwidth of 146 kHz, matrix of 128 × 128, FOV of 40 cm with one-half rectangular FOV technique, and NEX of 1. In this sequence, 90 and 180° radiofrequency (RF) pulse series were applied as well as two motion-probing gradients, one before and one after the 180° RF pulse. Motion-probing gradients were applied along all three directions: the slice-select, phase-encoding, and frequency-encoding directions. The strength of the motion-probing gradient was the same for the three directions, and the duration of the motion-probing gradient was 31 ms. A spectral spatial fat saturation RF pulse was used to exclude chemical shift artifacts. Diffusion sensitivity is governed by the gradient factor $b = g^2G^2d^2(D - d/3)$, where g is gyromagnetic ratio, G and d are, respectively, the strength and duration of the motion-probing gradient pulse, and D is the separation between the motion-probing gradient pulses. Diffusion-weighted single shot echo planar imaging by applying different three b values of 200, 400, and 600 s/mm^2 was performed during one breath-holding to exclude motion-induced artifacts (Figs. 1 and 2). In addition, gadolinium-enhanced T1-weighted MRI with fat suppression in the transverse and sagittal planes was performed in all patients.

Image Analysis

All images were reviewed on a workstation (Advantage Windows 3.1; GE). Circular regions of interests (ROIs) were placed within each cystic component that was ≥15 mm in diameter. When the regions appearing with various signal intensities of ≥15 mm in diameter were present in the same lobules on fat-suppressed T2-weighted images, each region was respectively evaluated. The outer margins of the ROIs were placed at least 3 mm away from the capsule, septa, and solid components that were defined as gadolinium-enhanced areas. Consequently, 66 components in 31 tumors were evaluated. The mean signal intensities of the cystic components of each lesion, subcutaneous fat tissue, and CSF in the lumbar spinal canal were measured on fat-suppressed T2-weighted images in the same sections as echo planar images. The mean signal intensities of the cystic components of each lesion, subcutaneous fat tissue, and psoas major muscle were measured on T1-weighted images with and without fat suppression. Because T1-weighted MRI was performed in a transverse plane, the ROIs on T1-weighted images were placed by means of a computer-navigated technique with T2-weighted imaging in the referred sagittal section on the workstation. In addition, the SDs of background signal intensity (SD_{air}) on T1- and T2-weighted images were obtained from an ROI in a phase-encoding direction outside the anterior abdominal wall.

Signal-to-noise ratios (SNRs) of each cystic component were calculated in all lesions in T1- and T2-weighted imaging by using the following formula: tumor $SNR = SI_{tumor}/SD_{air}$, where SI is signal intensity. Fat-suppressed indexes of each component of dermoid cysts were also calculated by using the following formula: fat-suppressed index = (SI_{tumor} on $fT1/SI_{muscle}$ on fT1)/(SI_{tumor} on $T1/SI_{muscle}$ on T1), where fT1 is fat-suppressed T1-weighted images, T1 is non-fat-suppressed T1-weighted images, and the subscript muscle refers to the psoas major muscle.

We calculated the ADCs with a set of echo planar images using a commercial program (Func-tool; GE).

We classified the signal intensities of each lesion into two ranks on non-fat-suppressed T1-weighted and fat-suppressed T2-weighted images. On non-fat-suppressed T1-weighted images, lesions with signal intensity that was equal to or lower than that of CSF were classified as hypointense and lesions with signal intensity that was higher than that of CSF as hyperintense. On T2-weighted

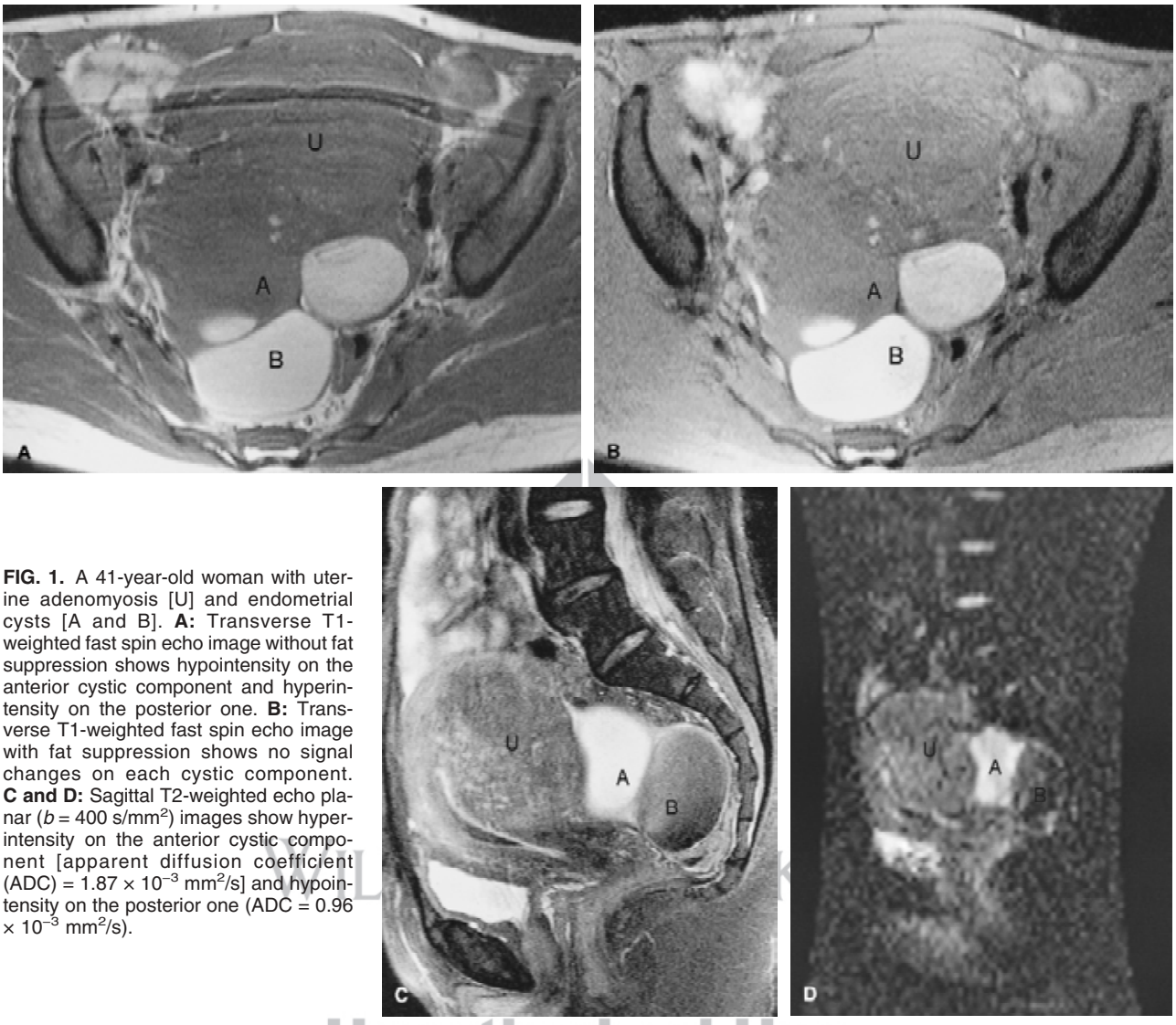

FIG. 1. A 41-year-old woman with uterine adenomyosis [U] and endometrial cysts [A and B]. **A:** Transverse T1-weighted fast spin echo image without fat suppression shows hypointensity on the anterior cystic component and hyperintensity on the posterior one. **B:** Transverse T1-weighted fast spin echo image with fat suppression shows no signal changes on each cystic component. **C and D:** Sagittal T2-weighted echo planar (b = 400 s/mm^2) images show hyperintensity on the anterior cystic component [apparent diffusion coefficient (ADC) = 1.87 × 10^{-3} mm^2/s] and hypointensity on the posterior one (ADC = 0.96 × 10^{-3} mm^2/s).

images with fat suppression, lesions with signal intensity that was lower than that of CSF were classified as hypointense and lesions with signal intensity that was equal to or higher than that of CSF as hyperintense. Consequently, we categorized all of the cystic components into four subgroups with signal intensities on T1- and T2-weighted images.

Furthermore, we classified the cystic components, which were histopathologically diagnosed as dermoid cyst, into three groups with the fat-suppressed index: well-fat-suppressed group (<0.5), intermediate-fat-suppressed group (≥0.5 and <0.9), and non-fat-suppressed group (≥0.9).

Statistical Analysis

The mean tumor SNRs on T1- and T2-weighted images and ADCs for each cystic component (more than four) were compared by using the Scheffé test, which is a one way analysis of variance. A p value of <0.05 was considered significant.

RESULTS

Tumor Characterization with ADC and T1- and T2-Weighted Imaging

On T1-weighted images, the mean SNR of endometrial cysts was highest and significantly differed from those of mucinous cystadenomas and malignant ovarian tumors ($p = 0.011$ and $p = 0.044$, respectively). The mean SNR of serous cystadenomas was lowest, although this was not statistically evaluated because of its small number of the cases (Table 1).

On T2-weighted images, the mean tumor SNR of dermoid cysts was significantly lower than those of mucin-

FIG. 2. A 46-year-old woman with mucinous cystadenoma of borderline malignancy. **A and B:** Transverse T1-weighted fast spin echo images with (B) and without (A) fat suppression show hypointensity on the huge cystic component. **C and D:** Sagittal T2-weighted fast spin echo image with fat suppression (C) and sagittal single-shot diffusion-weighted echo planar image (b = 400 s/mm^2) (D) show hyperintensity (apparent diffusion coefficient = 1.54 × 10^{-3} mm^2/s) on the huge cystic components.

ous cystadenomas and malignant ovarian tumors ($p = 0.005$ and $p = 0.001$, respectively). The mean tumor SNR of endometrial cysts showed no significant difference compared with mucinous cystadenomas and malignant ovarian tumors ($p = 0.439$ and $p = 0.390$, respectively) (Table 1).

In terms of the mean ADCs, it was not statistical different among the histopathologic groups; notably, the

TABLE 1. *T1SNRs, T2SNRs, and ADCs in each cystic ovarian component*

	No. of components	Diameter (cm)	T1SNR	T2SNR	ADC (10^{-3}/mm^2/s)
Endometrial cyst	18	5.3 ± 2.3	61.6 ± 23.9[a]	50.7 ± 26.3	1.24 ± 0.46
Dermoid cyst	29	4.1 ± 1.9	49.9 ± 29.6	32.7 ± 19.7[b]	1.27 ± 0.66
Serous cystadenoma	2	5.3 ± 4.8	10.0 ± 0.1	52.6 ± 1.6	1.64 ± 0.14
Mucinous cystadenoma	7	8.1 ± 5.9	22.6 ± 11.3[a]	66.2 ± 13.1[b]	1.61 ± 0.61
Malignant ovarian tumors	10	5.8 ± 3.2	32.6 ± 17.1[a]	65.1 ± 17.7[b]	1.64 ± 0.48

Numbers are means ± SD. T1SNR, signal-to-noise ratio on T1-weighted images; T2SNR, signal-to-noise ratio on T2-weighted images.

[a] $p < 0.05$, significant difference in T1SNR of endometrial cyst versus those of mucinous cystadenomas and malignant ovarian tumors.

[b] $p < 0.05$, significant difference in T2SNR of dermoid cysts versus those of mucinous cystadenomas and malignant ovarian tumors.

ADC, apparent diffusion coefficients.

mean ADCs of malignant ovarian tumors showed no significant difference compared with the others. The mean ADCs of endometrial cysts and dermoid cysts (1.24 and 1.27 × 10^{-3} mm^2 /s, respectively) were lower than those of serous and mucinous cystadenomas and malignant ovarian tumors (1.64, 1.61, and 1.64 × 10^{-3} mm^2/s, respectively). There were two cystic components >12 cm in diameter (one mucinous cystadenoma of 14.2 cm, the other mucinous cystadenoma of borderline malignancy of 18.5 cm). Their ADCs were 1.55 and 1.54 × 10^{-3} mm^2 /s, respectively (Table 1).

Relationship Between ADCs and T1- and T2-Weighted Imaging

In terms of endometrial cysts, 10 of 18 components were classified into the subgroup having hyperintensity on T1-weighted images and hypointensity on T2-weighted images. Four of 18 components were classified into the subgroup having typical watery intensity, hypointensity on T1-weighted images, and hyperintensity on T2-weighted images (Table 2). The mean ADC of the subgroup that showed typical watery intensity on conventional MR images was significantly higher than that of the subgroup of hyperintensity on T1-weighted images and hypointensity on T2-weighted images ($p = 0.008$) (Table 3; Fig. 3).

In terms of dermoid cysts, all of the well-fat-suppressed components were classified into the subgroup of hyperintensity on T1-weighted images and hypointensity on T2-weighted images. On the other hand, five of seven non-fat-suppressed components were classified into the subgroup that showed typical watery intensity on conventional MRI (Table 2). The mean ADC of the subgroup having typical watery intensity was higher than that of the others. In addition, the mean ADC of the non-fat-suppressed components was higher than that of the well-fat-suppressed components (Table 3).

Regarding serous cystadenomas, all of the two components were classified into the subgroup having hypointensity on T1-weighted images and hyperintensity on T2-weighted images. Regarding mucinous cystadenomas and malignant ovarian tumors, cystic components were classified into each subgroup (Table 3).

Among each histopathologic subgroup, the mean ADCs of lesions that showed typical watery intensities were similar, ranging from 1.54 to 1.84 × 10^{-3} mm^2 /s (Fig. 4). Furthermore, the SDs of dermoid cysts and malignant ovarian tumors were larger than those of other histopathologic subgroups.

DISCUSSION

The current study demonstrates a relationship between signal intensities in T1- and T2-weighted imaging and ADCs. The lesions showing typical watery intensity tended to have higher ADCs than the lesions showing atypical watery intensity on T1- and T2-weighted images. The differences in ADCs, therefore, were more closely related to the signal intensity of the fluid rather than a histopathologic group. The SDs of ADCs for each histopathologic group were large. Therefore, no useful information was added to diagnose cystic ovarian tumors.

There were some reports about the clinical application of diffusion-weighted imaging to diagnose cystic ovarian tumors (9–11). These authors reported that the cystic components of endometrial cysts and malignant ovarian tumors had lower ADCs than those of other lesions. In our study, the mean ADC of endometrial cysts was lower than that of serous and mucinous cystadenomas; however, no statistical differences were observed.

The signal intensities in T1- and T2-weighted imaging and ADCs are affected by protein concentrations, viscosity, magnetic susceptibility, and volume of H_2O (12,13). In our study, comparing the same histopathologic lesions in T2-weighted imaging, there was a tendency for lesions that showed hypointensity to have lower ADCs than the lesions that were hyperintense. Som and colleagues (14) reported the relationship between total protein concentrations and signal intensities in T1- and T2-weighted imaging. On T1-weighted imaging, 20–25% of proteins in solution showed high signal intensity. Less than 20% and higher than 25% of proteins in solutions showed low signal intensity. In T2-weighted imaging, >25% of proteins in solutions had low signal intensity. In our study, the cystic components that exhibited

TABLE 2. *Distribution of signal intensities of each component on T1- and T2-weighted images*

T1-weighted images	Hypointense		Hyperintense	
T2-weighted images	Hypointense	Hyperintense	Hypointense	Hyperintense
Endometrial cyst	0	4	10	4
Dermoid cyst	4	5	19	1
Fat-suppressed part	0	0	16	0
Equivocal	2	0	3	1
Non-fat-suppressed part	2	5	0	0
Serous cystadenoma	0	2	0	0
Mucinous cystadenoma	1	4	1	1
Malignant ovarian tumors	3	4	1	2

Numbers indicate numbers of components.

TABLE 3. *Relationship between apparent diffusion coefficients and signal intensities on T1- and T2-weighted images*

T1-weighted images	Hypointense		Hyperintense	
T2-weighted images	Hypointense	Hyperintense	Hypointense	Hyperintense
Endometrial cyst		1.78 ± 0.13[a]	1.01 ± 0.31[a]	1.34 ± 0.57
Dermoid cyst	1.66 ± 0.20	1.84 ± 0.34	1.00 ± 0.58	2.13
Fat-suppressed part			0.86 ± 0.29	
Equivocal	1.58 ± 0.30		1.70 ± 1.23	2.13
Non-fat-suppressed part	1.74 ± 0.05	1.84 ± 0.34		
Serous cystadenoma		1.64 ± 0.14		
Mucinous cystadenoma	1.40	1.73 ± 0.13	1.71	1.27
Malignant ovarian tumors	1.68 ± 0.68	1.54 ± 0.45	1.24	1.95 ± 0.42

Numbers are means ± SD.
[a] $p < 0.05$, significant difference between subgroups of endometrial cysts.

typical watery intensity on T1- and T2-weighted images had similar mean ADCs, ranging from 1.54 to 1.84 × 10^{-3} mm^2 /s, while it has been reported that the expected ADC of H_2O in the phantom at body temperature is 3.24 × 10^{-3} mm^2 /s (15). We speculate this discrepancy might be due to proteins in the fluid of cystic ovarian tumor. Some authors reported that the ADCs increased linearly with decreasing protein concentrations (16,17). In contrast to T1- and T2-weighted imaging, the ADC is sensitive to a small amount of protein. Some authors reported that the ADCs increased linearly with decreasing protein concentrations (16,17). Our result supported this theory to some extent.

Comparing the subgroups of endometrial cysts, the components that showed hyperintensity on T1-weighted images had lower ADCs than the components that showed hypointensity. We speculate this phenomenon would be caused by two factors: First, as the protein concentrations of the cystic components are increased up to 25%, their T1 values are shortened and ADCs are decreased. Second, endometrial cysts usually have bloody contents that contain some amounts of hemosiderin (18). Hemosiderin contains iron, a strong paramagnetic substance, which could shorten their T1 values and decrease their ADCs (19,20).

In our study, the mean ADCs of dermoid cysts were lower than those of mucinous cystadenomas and malignant ovarian tumors. The ADC of the fat-suppressed components was markedly decreased. However, this fact is a contentious issue. The cystic components of dermoid cysts contain various contents of fat. Because we per-

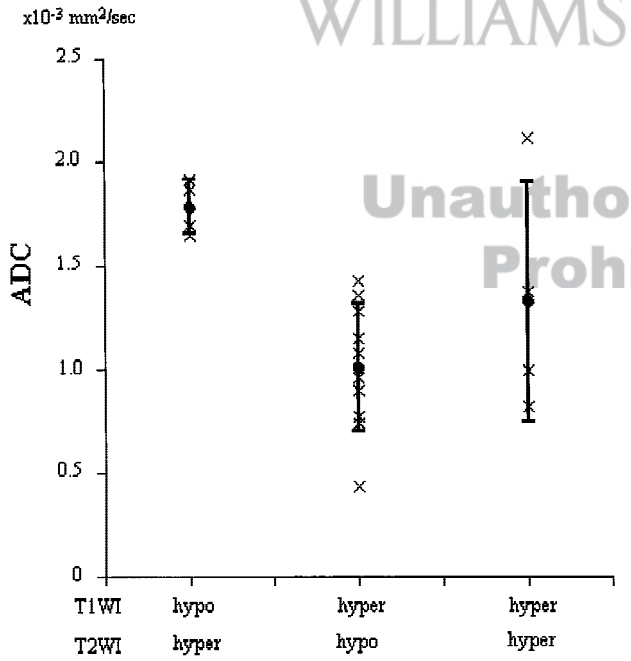

FIG. 3. Scatter-plots (Xs) of apparent diffusion coefficients of cystic components of endometrial cysts. Means (filled circles) and SDs are linked with a line. Hypo and hyper indicate hypointensity and hyperintensity on T1- and T2- weighted images, respectively.

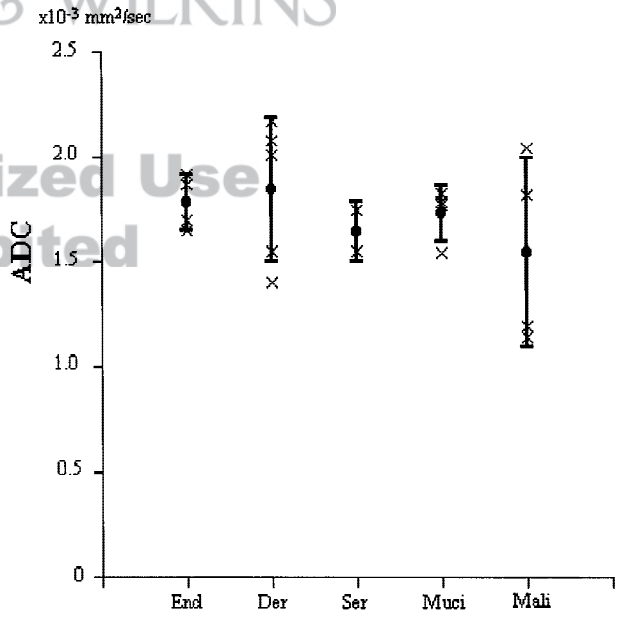

FIG. 4. Scatter-plots (Xs) of apparent diffusion coefficients of cystic components that showed typical watery intensities in T1- and T2-weighted imaging. Means (filled circles) and SDs are linked with a line. End, Der, Ser, Muci, and Mali indicate endometrial cysts, dermoid cysts, serous cystadenomas, mucinous cystadenomas, and malignant ovarian tumors, respectively.

formed diffusion-weighted imaging with echo planar sequence that used a spectral spatial fat saturation RF pulse, the signal intensities of fat were suppressed. Therefore, the measurements of the ADCs of fat-suppressed components became inaccurate.

In the group of malignant ovarian tumors, we could not find a clear relationship between signal intensities in T1- and T2-weighted imaging and the ADCs. In each subgroup classified with conventional MRI, the variance of the ADCs was large. We speculated this would result from their morphologic variety. Malignant ovarian tumors usually have some amounts of solids, hemorrhage, and other components in solution. Furthermore, necrotic tissue may sometimes be regarded as a cystic component even when contrast enhancement with gadolinium is performed.

We performed diffusion-weighted imaging with echo planar sequence. Because echo planar sequence is one of the most rapid imaging acquisitions, motion artifacts, which affect the quality of diffusion-weighted imaging, can be reduced. Furthermore, this sequence has good tissue contrast. However, the currently used diffusion-weighted images tend to be affected by susceptibility artifact and provides poor spatial resolution (21,22).

Our study had some limitations. The number of cases was small. The ADCs of the cystic components were variable among the same lesions and histopathologic groups. In previous reports, the highest and lowest ADCs of each component in the tumors were measured (9–11). Although this method was advantageous to distinguish endometrial cysts from other tumors, it is necessary to measure the ADCs repeatedly because of their large variance. Furthermore, many artifacts were present. By using the echo planar sequence, the ADCs could be inaccurate because of motion and susceptibility artifacts. It has been reported that lesions larger than 12 cm in diameter could have unrealistically high ADCs owing to the sloshing effect (11). In our study, however, two components of mucinous cystadenomas larger than 12 cm in diameter had ADCs of about 1.5×10^{-3} mm^2 /s. These values were slightly lower than the mean ADCs of mucinous cystadenomas. Consequently, these factors would cause the large variance and low reproducibility for the ADCs.

CONCLUSION

Although the ADC might provide other information, it is difficult to determine the threshold of the ADC for diagnosing cystic ovarian tumors because of their large variance. A tendency of ADCs could be speculated upon with T1- and T2-weighted imaging. We could not find additional clinical information with the ADC for diagnosing ovarian tumors.

REFERENCES

1. Mitchell DG, Mintz MC, Spritzer CE, et al. Adnexal masses: MR imaging observations at 1.5 T, with US and CT correlation. *Radiology* 1987;162:319–24.
2. Ghossain MA, Buy JN, Ligneres C, et al. Epithelial tumors of the ovary: comparison of MR and CT findings. *Radiology* 1991;181: 863–70.
3. Yamashita Y, Torashima M, Hatanaka Y, et al. Adnexal masses: accuracy of characterization with transvaginal US and precontrast and postcontrast MR imaging. *Radiology* 1995;194:557–65.
4. Hricak H, Mendelson E, Bohm-Velez M, et al. Role of imaging in cancer of the cervix. American College of Radiology. ACR appropriateness criteria. *Radiology* 2000;215:925–30.
5. Kinoshita T, Ishii K, Naganuma H, et al. MR findings of ovarian tumors with cystic components. *Br J Radiol* 2000;73:333–9.
6. Togashi K, Nishimura K, Kimura I, et al. Endometrial cysts: diagnosis with MR imaging. *Radiology* 1991;180:73–8.
7. Outwater E, Schiebler ML, Owen RS, et al. Characterization of hemorrhagic adnexal lesions with MR imaging: blinded reader study. *Radiology* 1993;186:489–94.
8. Le Bihan D, Breton E, Lallemand D, et al. MR imaging of intravoxel incoherent motions: application to diffusion and perfusion in neurologic disorders. *Radiology* 1986;161:401–7.
9. Moteki T, Ishizaka H, Horikoshi H, et al. Differentiation between hemangiomas and hepatocellular carcinomas with the apparent diffusion coefficient calculated from turboFLASH MR images. *J Magn Res Imag* 1995;5:187–91.
10. Moteki T, Ishizaka H. Evaluation of cystic ovarian lesions using apparent diffusion coefficient calculated from turboFLASH MR images. *Br J Radiol* 1998;71:612–20.
11. Moteki T, Ishizaka H. Evaluation of cystic ovarian lesions using apparent diffusion coefficient calculated from reordered turboFLASH MR images. *Magn Res Imag* 1999;17:955–63.
12. Le Bihan D, Turner R, Moonen CT, et al. Imaging of diffusion and microcirculation with gradient sensitization: design, strategy, and significance. *J Magn Res Imag* 1991;1:7–28.
13. Hashemi RH, William G. Bradley J. Tissue contrast: some clinical applications. In: *MRI: The Basics*. Baltimore: Williams & Wilkins, 1997:57–66.
14. Som PM, Dillon WP, Fullerton GD, et al. Chronically obstructed sinonasal secretions: observations on T1 and T2 shortening. *Radiology* 1989;172:515–20.
15. Muller MF, Prasad P, Siewert B, et al. Abdominal diffusion mapping with use of a whole-body echo-planar system. *Radiology* 1994;190:475–8.
16. Baranowska HM, Olszewski KJ. The hydration of proteins in solutions by self-diffusion coefficients. NMR study. *Biochim Biophys Acta* 1996;1289:312–4.
17. Brosio E, D'Ubaldo A, Verzegnassi B. Pulsed field gradient spin-echo NMR measurement of water diffusion coefficient in thickening and gelling agents: guar galactomannan solutions and pectin gels. *Cell Mol Biol* 1994;40:569–73.
18. Czernobilsky B. Endometriosis. In: Fox H, ed. *Haines and Taylor Obstetrical and Gynecological Pathology*. 3rd Ed. New York: Churchill Livingstone, 1987:763–817.
19. Nyberg DA, Porter BA, Olds MO, et al. MR imaging of hemorrhagic adnexal masses. *J Comput Assist Tomogr* 1987;11:664–9.
20. Hashemi RH, William G, Bradley J. Artifacts in MRI. In: *MRI: The Basics*. Baltimore: Williams & Wilkins, 1997:175–204.
21. Edelman RR, Wielopolski P, Schmitt F. Echo-planar MR imaging. *Radiology* 1994;192:600–12.
22. Niitsu M, Tanaka YO, Anno I, et al. Multishot echoplanar MR imaging of the female pelvis: comparison with fast spin-echo MR imaging in an initial clinical trial. *AJR* 1997;168:651–5.